

A Numerical Study of Convergence Speed in Solving Stress Field by Control Volume Based Finite Difference Method

Long Trandinh*

Hanoi University of Science and Technology, Ha Noi, Vietnam

*Corresponding author email: long.trandinh@hust.edu.vn

Abstract

The study presents an efficient implementation of the control volume-based finite difference method (CVFDM) integrated with a line-by-line solver for stress and strain analysis. The Navier's equation was discretized for each element, yielding fifteen displacement unknowns represented in a single equation. For this study, a three-unknown formulation per element was adopted. A line-by-line solver employing the TriDiagonal Matrix Algorithm (TDMA) was utilized to solve the equations. Dynamic memory allocation for updating displacements at previous element rows, enhancing convergence speed. Variables were solved and stored contiguously along a row in each time step, the iteration continued until the desired accuracy was achieved, eliminating the need for redundant boundary condition updates and reducing overall simulation time. A finite difference method (FDM)-based stress analysis application was developed based on the novel approach proposed in this work. Numerical simulations of three problems conducted using this application demonstrate a high level of agreement with theoretical solutions. The modified CVFDM with line-by-line solver proves to be an efficient and robust approach for stress and strain analysis, providing accurate and reliable results.

Keywords: CVFDM, stagger mesh, convergence criterion.

1. Introduction

In the context of displacement and stress analysis problems, researchers commonly initiate investigations by employing the finite element method (FEM) [1], or the utilization of renowned commercial software such as ANSYS or ABAQUS. Fluid flow simulations have typically employed finite difference method (FDM), as exemplified in mould filling simulations using SOLA_VOF [2,3] and investigations of bubble motion and local variables in multiphase flows using the volume of fluid (VOF) method [4], solved via control volume finite difference method (CVFDM). Stress analysis using the Finite Difference Method (FDM) typically follows a two-step process. First, the governing differential equation that describes the specific stress problem is formulated. Subsequently, this equation is discretized and solved numerically using FDM. Such as [5] problem of thermoelectricity for an infinitely long and isotropic circular cylinder of temperature dependent physical properties, the governing equation and boundary conditions were formulated in terms of differential equation, after that these equations were discretized and solved by FDM.

Yield and potential functions for plastic anisotropy, homogeneous anisotropic hardening were complicated differential equations [6]. The authors were using FDM combined algorithm loading-

unloading, loading-reloading, and deep-drawing/springback simulations to solve both first and second derivatives of yield function are approximated by central difference method. Also the finite difference formulation of Biot's theory has the properties of fourth order accuracy in space and second order accuracy in time combined with a parallel velocity-stress staggered-grid [7]. Besides, meshless generalized finite difference method (MGFDM) has been applied to analyse multi-layered composites, as demonstrated in [8] and [9], their applicability is often limited. These studies focused on situations where each layer possessed uniform material properties and homogeneous boundary conditions. In such scenarios, the MGFDM only exhibited good performance for rectangular models with multilayered materials. Casting simulations encompass a sequence of interrelated phenomena, including injection moulding, heat transfer, solidification, bubble dynamics, and residual stress. The results of each simulation step serve as input parameters for subsequent steps, coupling fluid flow and stress analysis.

To overcome this limitation, a novel hybrid approach [10] has been developed that synergistically integrates finite element method (FEM) and finite difference method (FDM) techniques, effectively combining the strengths of both methodologies. However, ensuring compatibility between FEM and

FDM presents challenges, such as connecting equilibrium and momentum equations and establishing compatible conditions for their respective meshes. These complexities can hinder automated design processes. For displacement and stress field problem solving via CVFDM coupled with staggered meshes [11] has proven effective. Surrounding a control volume element, six neighbouring elements are considered, with the choice of three, five, or seven unknowns depending on the solution form. The minimum number of unknowns equals the elements in a single mesh row. In this study, three unknowns were selected for model solving, and the TriDiagonal Matrix Algorithm (TDMA) was employed to solve the resulting equations. Methods to accelerate convergence rate and reduce simulation time are explored and discussed.

2. Governing Equations

To numerically solve the stress field problem, the differential equilibrium equations were discretized on a staggered mesh. The stress-strain relationship was incorporated via Hooke's law, substituting strains for stresses in the equilibrium equations. Subsequently, strain variations were expressed in terms of displacements through Cauchy's equations. This resulted in the discretization of the differential equilibrium equations in terms of displacements for each element of the staggered mesh. The discretized equations and the corresponding unknowns are presented in following sections:

2.1. Differential Equilibrium Equations (Navier Equations)

$$\frac{\partial \sigma_{ij}}{\partial x_i} + p_i = 0 \quad (1)$$

in which σ_{ij} represent for stress in an element, x_i is direction x , y or z and p_i is force per unit volume.

Discretization of the first equilibrium equation (direction x)

The equilibrium in (1) are represented for the three coordinate directions (x , y , z), which exhibit mathematical similarities. To minimize the number of equations presented, only the x -direction equilibrium equation was discretized explicitly. To represent the remaining equilibrium equations, subscripts and superscripts in the x -direction equation were substituted with their corresponding y - and z -direction counterparts. The discretization of the first equilibrium equation was conducted using a staggered mesh. Normal stresses were positioned at the centre of control volumes, while shear stresses were located at the edges (Fig. 1). This discretization was applied to ensure equilibrium between adjacent elements.

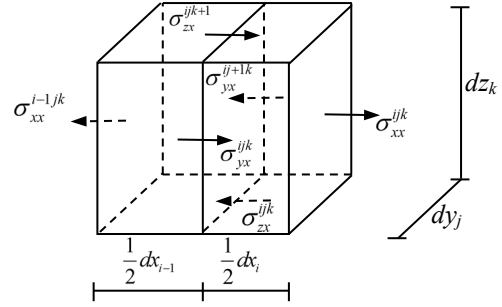


Fig. 1. The equilibrium of stresses on control volume element

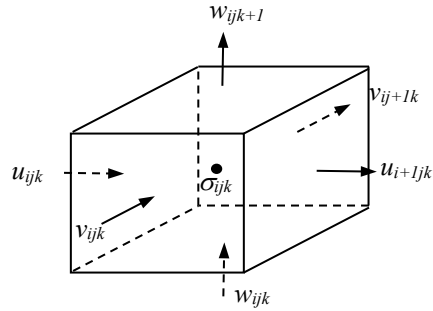


Fig. 2. Normal stress on control volume

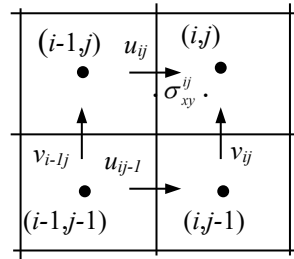


Fig. 3. Shear stress on control volume

$$\frac{\sigma_{xx}^{ijk} - \sigma_{xx}^{i-1,jk}}{\frac{1}{2}(dx_{i-1} + dx_i)} + \frac{\sigma_{yx}^{ij+1,k} - \sigma_{yx}^{ijk}}{dy_j} + \frac{\sigma_{zx}^{ijk+1} - \sigma_{zx}^{ijk}}{dz_k} + \frac{dx_{i-1}p_x^{i-1,jk} + dx_i p_x^{ijk}}{dx_{i-1} + dx_i} = 0 \quad (2)$$

In Equation (2), each stress component, expressed in terms of displacements and temperature, was discretized over control volumes. The normal stress was located at the centre of a control volume (Fig. 2), while the shear stresses were positioned on the edges connecting four surrounding finite elements (Fig. 3).

The discretization of the normal stress specifically took the following form:

$$\sigma_{xx}^{ijk} = \frac{u_{i+1jk} - u_{ijk}}{Mx_{ijk}} + \frac{v_{ij+1k} - v_{ijk}}{Mvy_{ijk}} + \frac{w_{ijk+1} - v_{ijk}}{Mvz_{ijk}} - K_{ijk} \Delta T \quad (3)$$

in which

$$Mx_{ijk} = \frac{dx_i}{\frac{E_{ijk}}{1+\nu_{ijk}} \left(1 + \frac{\nu_{ijk}}{1-2\nu_{ijk}}\right)} \quad (4)$$

$$Mvy_{ijk} = \frac{dy_j}{\frac{E_{ijk}}{1+\nu_{ijk}} \frac{\nu_{ijk}}{1-2\nu_{ijk}}} \quad (5)$$

$$Mvz_{ijk} = \frac{dz_j}{\frac{E_{ijk}}{1+\nu_{ijk}} \frac{\nu_{ijk}}{1-2\nu_{ijk}}} \quad (6)$$

$$K_{ijk} = \frac{E_{ijk} \alpha_{ijk}}{1-2\nu_{ijk}} \quad (7)$$

2.2. Discretization of Shear Stress

$$\sigma_{xy}^{ijk} = \frac{u_{ijk} - u_{i-1k}}{2} \left(Mxy_{ijk} + Mxy_{ij-1k} \right) + \frac{v_{ijk} - v_{i-1jk}}{2} \left(Myx_{ijk} + Myx_{i-1jk} \right) \quad (8)$$

in which

$$Mxy_{ijk} = \frac{dy_j}{\frac{E_{i-1jk}}{2(1+\nu_{i-1jk})} dx_{i-1} + \frac{E_{ijk}}{2(1+\nu_{ijk})} dx_i} \quad (9)$$

$$Myx_{ijk} = \frac{dx_i}{\frac{E_{ij-1k}}{2(1+\nu_{ij-1k})} dy_{j-1} + \frac{E_{ijk}}{2(1+\nu_{ijk})} dy_j} \quad (10)$$

The material constants in mentioned equation included modulus of elasticity E , Poisson's ratio ν , heat conductivity coefficient α and temperature T .

The discretization stresses within the staggered mesh enabled the representation of thermo-mechanical stresses in the casting process. This facilitated the analysis of the stress field at the interface of dissimilar materials, such as the mould-die interface.

The stresses were discretized in equations (3) and (8) for substitution into equation (2). The first equilibrium equation in terms of displacement has been simplified and is expressed as follows:

$$a_{p1}^{ijk} u_p = a_{w1}^{ijk} u_w + a_{e1}^{ijk} u_e + a_{s1}^{ijk} u_s + a_{n1}^{ijk} u_n + a_{b1}^{ijk} u_b + a_{t1}^{ijk} u_t + b_1^{ijk} \quad (11)$$

in which the subscripts were presented for elements: pole "p", west "w", east "e", north "n", south "s", top "t" and bottom "b".

3. Equivalent Shear Stress

Shear stresses are applied to the sides of the element, while normal stress is applied to the central point, as shown in Fig. 4. Plasticity theories require equivalent total stress at a single point.

To account for the shear stresses, a formula is needed to transform them into shear stress at the central point. The average shear stress at the central point is calculated as follows:

$$\bar{\sigma}_{xy}^{ijk} = \frac{1}{4} \left(\sigma_{xy}^{ijk} + \sigma_{xy}^{i+1jk} + \sigma_{xy}^{ij+1k} + \sigma_{xy}^{i+1j+1k} \right) \quad (12)$$

in which $\bar{\sigma}_{xy}^{ijk}$ is the equivalent shear stress at the central, shear stresses at four sides of the element "ijk" shown as shear stresses at four corners of planar element in Fig 4.

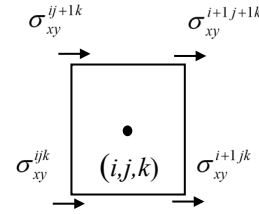


Fig. 4. Equivalent shear stress at the central

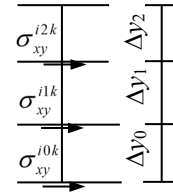


Fig. 5. Shear stress on boundary

The characteristic of shear stress is applied to the sides of elements. It is influenced by the displacements of four neighbouring elements (as in 8). If any of these four elements are absent, their displacements are set to zero. This situation arises when shear stress is applied to an external face of a boundary element. As a result, the absolute value of these shear stresses may increase unexpectedly, significantly impacting the equivalent shear stress and equivalent total stress of the boundary element. To address this issue, several approaches are available. One option involves ignoring shear stresses on the boundary when calculating the equivalent shear stress.

$$\bar{\sigma}_{xy}^{ijk} = \frac{1}{\left(\delta^{ijk} + \delta^{i+1jk} + \delta^{ij+1k} + \delta^{i+1j+1k} \right)} \left(\delta^{ijk} \sigma_{xy}^{ijk} + \delta^{i+1jk} \sigma_{xy}^{i+1jk} + \delta^{ij+1k} \sigma_{xy}^{ij+1k} + \delta^{i+1j+1k} \sigma_{xy}^{i+1j+1k} \right) \quad (13)$$

where:

$$\delta^{ijk} = \begin{cases} 0 & \text{if } \sigma^{ijk} \text{ on boundary} \\ 1 & \text{if } \sigma^{ijk} \text{ not on boundary} \end{cases} \quad (14)$$

An alternative approach is to calculate the shear stresses at the boundary through linear extrapolation from the internal shear stresses shown in Fig. 5.

$$\sigma_{xy}^{i0k} = \sigma_{xy}^{i1k} \cdot \frac{\Delta y_0 + \Delta y_1}{\Delta y_1} - \sigma_{xy}^{i2k} \frac{\Delta y_0}{\Delta y_1} \quad (15)$$

in which σ_{xy}^{i0k} is shear stress at the boundary, σ_{xy}^{i1k} , σ_{xy}^{i2k} are internal shear stresses.

In the evaluation of equivalent shear stress, shear stress can be disregarded or estimated indirectly through linear extrapolation. The latter approach, while slightly more accurate, relies on the adequacy of four stress components in the equivalent shear stress formulation.

The difference in accuracy between the two options is negligible. Equivalent shear stress can be conceptualized as the average of the trapezoidal region bounded by the shear stresses inside and on the boundary. The first option discards one of the bottom rows, reducing the average to the remaining row. If the two bottom rows are identical, the results from both options converge.

In practice, the difference in shear stresses between the two options is minimal, unless the mesh is excessively coarse.

4. Line-By-Line Solver

The equilibrium equations comprise 15 displacement unknowns along each directional component. Simultaneous resolution of all unknowns presents significant challenges due to the complexity of the system. Consequently, the equations are solved independently and sequentially on a line-by-line basis, which simplifies the solution process.

The numerical solver employs a line-by-line method that combines the iterative Gauss-Seidel method with TDMA. This approach is referred to as the Line Gauss-Seidel (LGS) Method [12]. TDMA method is particularly well-suited for solving one-dimensional problems, where the Navier equations result in a tridiagonal coefficient matrix. This structure allows for direct solution through forward and backward substitution, considerably simplifying the process.

TDMA was employed to solve the equilibrium equations in each spatial direction independently. In the x -direction, the traversal direction was selected, while the y - and z -directions were treated as sweep directions. Consequently, displacements at points "w" (west), "p" (pole), and "e" (east) in the x -direction became variables, while displacements at points "n" (north), "s" (south), "t" (top), and "b" (bottom) were treated as parameters or constants in the equation. Similar approaches were applied to the remaining equilibrium equations. The equations were

subsequently transformed into tridiagonal linear algebraic equations.

The x -direction cross direction in the first equilibrium equation.

$$-a_{w1}^{ijk} u_w + a_{p1}^{ijk} u_p - a_{e1}^{ijk} u_e = a_{s1}^{ijk} u_s + a_{n1}^{ijk} u_n + a_{b1}^{ijk} u_b + a_{t1}^{ijk} u_t + b_1^{ijk} \quad (16)$$

The y -direction cross direction in the second equilibrium equation.

$$-a_{s2}^{ijk} v_s + a_{p2}^{ijk} v_p - a_{n2}^{ijk} v_n = a_{w2}^{ijk} v_w + a_{e2}^{ijk} v_e + a_{b2}^{ijk} v_b + a_{t2}^{ijk} v_t + b_2^{ijk} \quad (17)$$

The z -direction cross direction in the second equilibrium equation.

$$-a_{b3}^{ijk} w_b + a_{p3}^{ijk} w_p - a_{t3}^{ijk} w_t = a_{w3}^{ijk} w_w + a_{e3}^{ijk} w_e + a_{s3}^{ijk} w_s + a_{n3}^{ijk} w_n + b_3^{ijk} \quad (18)$$

5. Convergence Criteria

Traditional convergence criteria in iterative solvers for displacement field problems typically measure the residual values between successive iterations. However, this approach presents a limitation when handling problems with both large and small displacements.

In large displacement problems, a tolerance of approximately 0.01 is generally sufficient to obtain accurate results. Conversely, small displacement problems with maximum displacement values on the order of 0.01 mm require tolerances below 10^{-5} for accuracy.

Applying a fixed tolerance for all problems can lead to incorrect results. If the tolerance is based on large displacement problems, it may be too coarse for small displacement problems, resulting in premature termination of iterations before sufficient convergence is achieved. On the other hand, if the tolerance is based on small displacement problems, it may be overly stringent for large displacement problems, leading to unnecessary computation time.

For instance, in a large displacement problem, residual values around 0.01 may be acceptable for accuracy. The iteration may halt and produce a solution, but excessive computational time is spent reducing the residuals from 0.01 to 10^{-5} , which may not be necessary. Table 1 demonstrates this issue, where the unnecessary computation time can be ten times longer than required.

Table 1. Relative tolerance

Tolerance	Number of Iteration-step
0.001	490
0.0001	4940
0.00001	28100

To address both issues, a substitute convergence criterion is required. Calculating residual values as a percentage ratio between the residual displacement value between two consecutive steps and the displacement on one mesh element provides a solution. Utilizing a percentage ratio ensures that this criterion is independent of the model's size or displacement level.

$$r_u(i, j, k) = \left| \frac{u_{ijk}^s - u_{ijk}^{s-1}}{\Delta u_{\max}^s} \right| \cdot 100\% \quad (19)$$

$$r_u = \max(r_u(i, j, k)) \quad (20)$$

in which s is iteration step, Δu_{\max}^s is maximum displacement on a single mesh. u_{ijk}^s is displacement at current iteration step and u_{ijk}^{s-1} is displacement at previous iteration step.

Similarity residuals for the y direction and z direction are r_v and r_w .

The final residual can be calculated as

$$r = \max(r_u, r_v, r_w) \quad (21)$$

6. Convergence Speed and Simulation Duration

Each of equilibrium equations (16), (17), (18) governing displacements in the x , y , and z directions incorporates seven displacement unknowns. These unknowns include one central displacement and six displacements on the element's six faces. While solving for all seven unknowns simultaneously would theoretically yield the fastest convergence, a reduction to five or even three unknowns is possible. However, increasing the number of unknowns necessitates the establishment of more complex boundary conditions. For instance, employing a five-unknown system requires five boundary conditions per equation. These conditions involve specifying both the first and last terms in each row (resulting in two conditions) and imposing three additional conditions on directions perpendicular to the specified terms. While achievable for specific models, this approach becomes cumbersome for general applicability. Furthermore, it presents software usability challenges, as users would need to declare a greater number of parameters to establish sufficient boundary conditions for diverse problems.

Due to its ease of implementing boundary conditions and universal applicability to various computational models, the 3-unknown formulation is the most widely adopted approach. In theory, all 3-unknown models exhibit equivalent convergence rates per iteration for the displacement being solved. However, within a 3D problem, the convergence speed in a particular direction is influenced by the remaining two directions. Additionally, the convergence of a specific row is impacted by the previous row. This interplay between rows becomes crucial for optimizing

overall convergence speed. It's noteworthy that setting up boundary conditions often consumes a significant portion of the entire simulation process. While employing a higher number of boundary conditions enhance convergence per iteration, it doesn't necessarily translate to a reduction in total computation time. This section will delve deeper into these considerations.

In the application of the Line Gauss-Seidel method to solve equilibrium equations, the displacements on the current row are updated immediately upon solving the tridiagonal equations for that row. This approach facilitates the convergence of displacements on subsequent rows, potentially accelerating the convergence of the entire system for one- or two-dimensional problems. However, challenges arise when applying this method to three-dimensional problems. The immediate update of displacements on the current row can introduce difficulties.

At the current stage, prior to the solution of the equations represented in this row, all displacements retain their previous values and are depicted as solid circles in Fig. 6. Upon solving the equations, the displacements are updated with new values, represented by hollow circles at points " w ", " P ", and " e ". In the next step, the displacements at " w ", " P ", and " e " have been freshly updated and correspond to the displacements at points " s ". The disparity between the values at points " s " and " n " accelerates the convergence of displacements at points " w ", " P ", and " e " relative to those at points " w ", " P ", and " e ". However, this update procedure also introduces slippage between the rows. While this update process initially enhances convergence speed, it is only evident during the initial iteration steps. When the solution process progresses sequentially in the x , y , and z directions, the slippage accumulates in the x and y directions. This phenomenon not only diminishes convergence speed in the z direction but also compromises the accuracy of displacements along this direction.

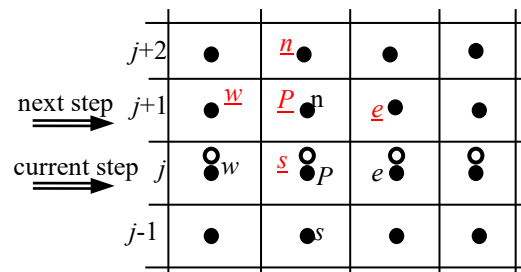


Fig. 6. Slippage in solving row

A novel approach for variable storage in the solution of systems of equations is proposed. By utilizing a single auxiliary variable to store intermediate solution values, the slide is eliminated, and convergence is significantly accelerated. Table 2

demonstrates the improved performance of this approach. However, it requires additional memory due to the introduction of the auxiliary variable. Therefore, the recommended practice is to use a variable of the same size as the displacement variables (u , v , or w) to minimize memory requirements. This variable can be reused for each directional component of the displacement solution.

Table 2. Tolerance for old and novel methods

Iteration step	Tolerance % (old method)	Tolerance % (novel approach)
1	100.0	100.0
2	33.003	38.198
3	16.177	30.582
4	12.464	18.073
5	11.840	12.475
6	11.340	10.166
7	10.886	8.368
50	5.370	0.982
100	3.937	0.490
500	1.880	0.098
1000	1.361	0.049
1500	1.127	0.032

The traditional numerical method for solving the equilibrium equations in a finite differential analysis involves employing two three-dimensional arrays of static memory. The first array stores the displacements obtained from the previous iteration, while the second array contains the updated displacements after solving for all elements in three directions during the current iteration. Following the solution process, the displacements in the second array are compared with those in the first array to determine the tolerance achieved for that iteration. Subsequently, the updated displacements from the second array are transferred to the first array, overwriting the previous results, and serving as the basis for subsequent iterations.

A novel computational method is introduced that utilizes a single three-dimensional static memory array to store displacement results. Additionally, a one-dimensional dynamic memory array was employed to store new displacements on the current solution row. Displacements in dynamic memory were compared with those in the static memory to obtain a tolerance value. Upon comparison, the results in the dynamic memory are immediately updated into the static memory. This continuous update of new results at row j (depicted as hollow circles in Fig. 6) enhances the accuracy of the displacement values at row $j + 1$. This is achieved by utilizing new data from row j and old data from row $j + 1$ and row $j + 2$, rather than relying solely on old data for all three rows.

Furthermore, the proposed method offers a significant memory economy compared to the classical method, as it employs only one three-dimensional array instead of two.

To accelerate the convergence of the computational problem, an analysis of the time expenditure at each calculation step was conducted. For a single-material model, results revealed that established equation includes setting boundary conditions and assigned material properties for each component (encompassing 15 variables per row) accounted for 86% of the computational time, equation solving and memory updates consumed approximately 13% and less than 1%, respectively. Furthermore, the simulation time for the multi-material model was significantly longer (approximately 10 times) compared to the single-material model. This disparity emerged despite the identical geometric configuration, boundary conditions, and mesh topology between the two models. Analysis revealed that the time-consuming aspect resided primarily in the assignment of boundary conditions and material properties, which accounted for over 98% of the modelling duration for the multi-material model.

To achieve computational efficiency, variables should be solved and stored contiguously along a row in each time step. Once the row satisfies the desired accuracy criteria, the computation proceeds to the next row. This iterative process avoids multiple boundary condition updates, thereby accelerating the convergence rate and simulation time.

7. Numerical Models

The KH stress application was developed based on the mentioned calculation methodology for stress and displacement analysis. Subsequently, numerical simulations were performed using the KH stress application, and the results exhibited a high degree of consistency with theoretical predictions, as demonstrated in the following:

Model 1. A Tensile Bar

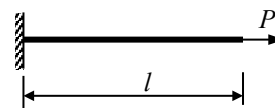


Fig. 7 A tensile bar

A fixed steel bar with a square cross section of 20×20 mm is subjected to a uniform load of intensity $p = 10^8$ Pa (see Fig. 7). The bar has length of $L = 1$ m, modulus of elasticity $E = 2 \times 10^{11}$ Pa and Poisson's ratio $\nu = 0.3$.

- *Theoretical result:*

$$\sigma_{yy} = \sigma_{zz} = 0; \sigma_{xx} = 10^8 \text{ Pa};$$

$$\text{Von_Mises stress: } \sigma_{vm} = \sigma_{xx} = 10^8 \text{ Pa}$$

Strain:

$$\varepsilon_{xx} = \frac{\sigma_{xx}}{E} = 0.5 \times 10^{-3}$$

$$\varepsilon_{yy} = \varepsilon_{zz} = \nu \frac{\sigma_{xx}}{E} = 0.15 \times 10^{-3}$$

- Numerical result by KH stress application.

The mesh system for the problem: $20 \times 4 \times 4$ mesh eyes $\Delta x = \Delta y = \Delta z = 5 \text{ mm}$

Displacements on one mesh eye

$$u = 2.4927e-3 \text{ mm}$$

$$v = 0.748e-3 \text{ mm}$$

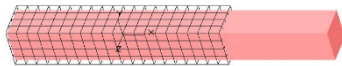
$$w = 0.7478e-3 \text{ mm}$$

$$\varepsilon_{xx} = \frac{u}{\Delta x} = \frac{2.4927}{5} e-3 = 0.4985e-3$$

$$\varepsilon_{yy} = \frac{v}{\Delta y} = \frac{0.748}{5} e-3 = 0.1496e-3$$

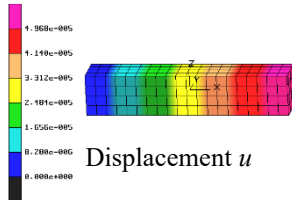
$$\varepsilon_{zz} = \frac{w}{\Delta z} = \frac{0.7478}{5} e-3 = 0.14956e-3$$

Von_Mises Stress: $\sigma_{vm} = 9.97e7 \text{ Pa}$, the error of stress is 0.3%.



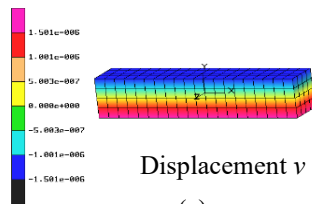
Deformation

(a)



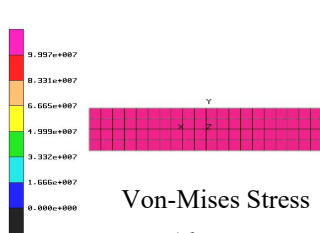
Displacement u

(b)



Displacement v

(c)



Von-Mises Stress

(d)

Fig. 8. Numerical results by KH stress application, (a) deformation model, (b) Contour of displacement in x direction, (c) Contour of displacement in y direction, and (d) Contour of Von_Mises stress of bar.

Model 2. A Square Plate with a Central Hole

A square plate with dimensions of $1.0 \text{ m} \times 1.0 \text{ m}$ plate and a thickness of $t = 0.1 \text{ m}$ was fabricated from steel. A central hole of diameter $d = 0.4 \text{ m}$ was bored into the plate. The steel exhibited material properties of elastic modulus $E = 2 \times 10^{11} \text{ Pa}$ and Poisson's ratio, $\nu = 0.3$. A vertical tensile load in the form of a pressure $p = 100 \text{ MPa}$ was applied along the horizontal side of the plate (as depicted in Fig. 9)

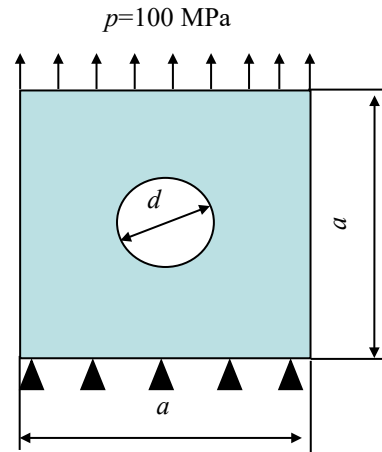


Fig. 9. A square plate with central hole subjected to vertical tensile load

- Theoretical result

Kirsch's solution for stresses at a hole are for the case of uniaxial tension in an infinite plate. Uniaxial tension is represented by the remote stress, σ_{∞} . The hole has radius, a , the radial coordinate is r (which is meaningless when $r < a$), and $\theta = 0$ aligns with the remote loading direction. The solution for the stress state around a hole is

$$\sigma_{rr} = \frac{\sigma_{\infty}}{2} \left(1 - \left(\frac{a}{r} \right)^2 \right) + \frac{\sigma_{\infty}}{2} \left(1 - 4 \left(\frac{a}{r} \right)^2 + 3 \left(\frac{a}{r} \right)^4 \right) \cos 2\theta$$

$$\sigma_{\theta\theta} = \frac{\sigma_{\infty}}{2} \left(1 + \left(\frac{a}{r} \right)^2 \right) - \frac{\sigma_{\infty}}{2} \left(1 + 3 \left(\frac{a}{r} \right)^4 \right) \cos 2\theta$$

$$\sigma_{r\theta} = -\frac{\sigma_{\infty}}{2} \left(1 + 2 \left(\frac{a}{r} \right)^2 - 3 \left(\frac{a}{r} \right)^4 \right) \sin 2\theta$$

The stress concentration at the hole occurs $\theta = \pm 90^\circ$ depicted as pink region and minimum stress with $\theta = 0^\circ$ or 180° represented blue region in Fig. 10 (b) and (c)

- Numerical result by KH stress application

The numerical results obtained through the KH stress application, as depicted in Fig. 10, exhibit substantial agreement with theoretical predictions.

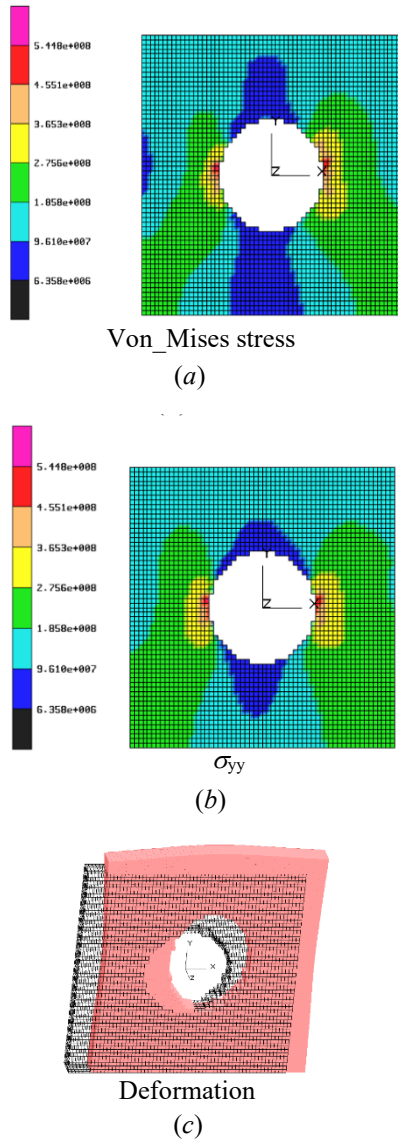


Fig. 10 Numerical results (a) Von_Mises stress contour, (b) contour of stress on y direction, and (c) deformation model.

Model 3. A Rectangular Plate with a Central Hole

A rectangular steel plate with dimensions of width $b = 1.0$ m, length $a = 4.0$ m, and thickness $t = 0.1$ m contains a central circular hole with diameter $d = 0.2$ m. The material properties of the plate are elastic modulus $E = 2 \times 10^{11}$ Pa and Poisson's ratio $\nu = 0.3$. Vertical horizontal loading in the form of a pressure $p = 10^6$ Pa is applied along the vertical side of the plate, see Fig. 11 (a).

- Numerical Modelling

Due to symmetry about the horizontal axes, a quarter of the plate was used for numerical modelling to reduce computational complexity. This approach assumes symmetric deformation and stress distribution in the entire plate, see Fig. 12 (b).

- Numerical result by KH stress application

The stress concentration at the hole occurs $\theta = \pm 90^\circ$ depicted as dark grey region and minimum stress with $\theta = 0^\circ$ or 180° represented deep black region in Fig. 12 (a).

The numerical results obtained through the KH stress application, as depicted in Fig. 12, exhibit substantial agreement with theoretical predictions.

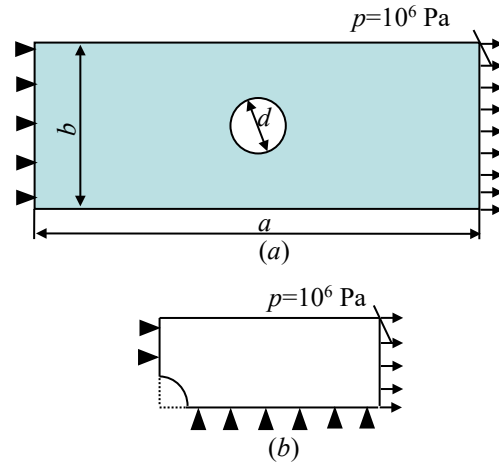


Fig. 11. (a) A rectangular plate with central hole subjected to horizontal load, (b) A quarter of the plate for numerical model.

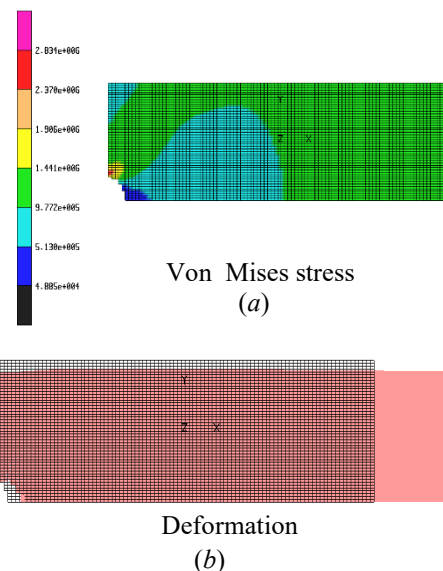


Fig. 12 (a) Von Mises stress contour and (b) displacement of a quarter of the plate with central hole

8. Conclusion

Control volume base finite different method has been proposed for the solution of displacement and stress field problems in multi-material solids. The accuracy of total stress, represented by the von Mises stress, on boundary elements has been improved by

employing a modified formula for shear stress. A line-by-line solver employing TDMA was utilized to solve the equations. Dynamic memory allocation for updating displacements at previous element rows, enhancing convergence speed. Variables were solved and stored contiguously along a row in each time step, the iteration continued until the desired accuracy was achieved, eliminating the need for redundant boundary condition updates, and reducing overall simulation time.

FDM-based stress analysis application was developed based on the novel approach proposed in this work. Numerical simulations of three problems conducted using this application demonstrate a high level of agreement with theoretical solutions.

Acknowledgement

The KH stress application utilizes the sole main process for stress and displacement analysis. Input data preparation, mesh generation and display of stress and displacement outputs were facilitated by the ZCAST software development team at Korea Institute of Industrial Technology (KITECH). The author gratefully acknowledges the support of the ZCAST team for their invaluable contributions to this work.

References

- [1] K-J. Bathe, and E L. Wilson, Numerical Method in Finite Element Analysis, Prentice Hall Inc, N.J, 1976, pp. 528.
- [2] S.D. Elliot, Fluid flow aspects of solidification modeling: Simulation of low pressure die casting, Ph.D. Thesis, Department of Mining & Metallurgical Engineering, The University of Queensland, 2000.
- [3] R. BaBaei, H. Esaellian, N. Varahram, and P. Davami, Mathematical and computational modeling of mould filling and heat transfer metal casting, Iranian Journal of science and technology, vol. 29, no. B5, 2005.
- [4] Y. Wenqi, L. Suiqing, L. Shuping, T. Tao, and X. Kunlun, Numerical simulation of bubble motion in horizontal reducer pipelines, Engineering Applications of Computational Fluid Mechanics, vol. 5, iss. 4, 2011, pp. 517-529.
<https://doi.org/10.1080/19942060.2011.11015391>
- [5] A.M. Farhan, A.M. Abd-Alla, Moaiad A. Khder, Solution of a problem of thermal stresses in a non-homogeneous thermoelastic infinite medium of isotropic material by finite difference method, Journal of Ocean Engineering and Science, vol. 4, iss.3, Sep. 2019, pp. 256-262.
<https://doi.org/10.1016/j.joes.2019.05.001>
- [6] Hyunsung Choi, Jeong Whan Yoon, Stress integration-based on finite difference method and its application for anisotropic plasticity and distortional hardening under associated and non-associated flow rules, Computer Methods in Applied Mechanics and Engineering, vol. 345, Mar. 2019, pp. 123-160.
<https://doi.org/10.1016/j.cma.2018.10.031>
- [7] Dong-Hoon Sheen, Kagan Tuncay, Chang-Eob Baag, Peter J. Ortoleva, Parallel implementation of a velocity-stress staggered-grid finite-difference method for 2-D poroelastic wave propagation, Computers & Geosciences, vol. 32, iss. 8, Oct. 2006, pp. 1182-1191.
<https://doi.org/10.1016/j.cageo.2005.11.001>
- [8] Wang Yuanyuan, Gu Yan, Fan Chia-Ming, Chen Wen, Zhang Chuanzeng, Domain-decomposition generalized finite difference method for stress analysis in multi-layered elastic materials, Engineering Analysis with Boundary Elements, vol. 94, Sep. 2018, pp. 94-102.
<https://doi.org/10.1016/j.enganabound.2018.06.006>
- [9] Yuanyuan Wang, Yan Gu, Jianlin Liu, A domain-decomposition generalized finite difference method for stress analysis in three-dimensional composite materials, Applied Mathematics Letters, vol. 104, Jun. 2020, pp. 106226.
<https://doi.org/10.1016/j.aml.2020.106226>
- [10] S. Ho-Mun, C. Chongdu, and K. Si-Young, A hybrid method for casting process simulation by combining FDM and FEM with an efficient data conversion algorithm, Journal of Materials Processing Technology, vol. 133, iss. 3, Feb. 2003, pp. 311-321.
[https://doi.org/10.1016/S0924-0136\(02\)01008-7](https://doi.org/10.1016/S0924-0136(02)01008-7)
- [11] E. Robert, G. Thierry, and H. Raphaele, Finite volume methods, P.G. Ciarlet, J.L. Lions eds, vol. 7, 1997, pp. 713-1020.
- [12] J. Rigola, C. D. Perez-Segarra, A. Oliva, J. M. Serra, M. Escriba, and J. Pons, Advanced numerical simulation model of hermetic reciprocating compressors, Parametric study and detailed experimental validation. in International Compressor Engineering Conference, Purdue University, USA, 2000, pp. 23-30.